Transactions of the **14th International Conference on Structural Mechanics in Reactor Technology** (SMiRT 14), Lyon, France, August 17-22, 1997 **F03B/1**

Dynamic buckling experiments of fluid-structure coupled co-axial thin cylinders

Fukuyama M.[1], **Nakagawa M.**[1], **Ishihama K.**[2], **Hagiwara Y.**[3], **Toyoda Y.**[3]
(1) Hitachi Ltd, Japan
(2) Hitachi Works, Hitachi Ltd., Japan
(3) Central Research Institute of Electric Power Industry, Japan

ABSTRACT : Dynamic buckling experiments of thin cylindrical shells placed inside of a rigid liquid container with a narrow fluid gap which represens the thermal baffles and the reactor vessel of a FBR were performed using a shaking table. The fluid pressure caused by the vibration of fluid-structure acts upon shells and it causes buckling deformation on them. The mode of buckling observed is similar to that predicted by static analysis, which is one of the external pressure buckling. The buckling strength is clarified with different types of test cylinder under different excitation waves. The buckling pressure is predicted by static buckling analysis.

INTRODUCTION

The main vessel and other important components of FBRs must have thin shell structures in order to withstand severe thermal conditions. Consequently, one of the most critical factors in earthquake resistant FBR design is the prevention of buckling. The Central Research Institute of Electric Power Industry and nuclear power plant makers have been working together on a project to research the buckling strength of FBR structures commissioned by the Ministry of International Trade and Industry of Japan.

Much of the research concerning the shear-bending buckling of short cylindrical shells has been completed in this project and a seismic buckling design outline which mainly concerns the main vessels of FBR has been established. [1][2] Following this project, the buckling of important components of FBR other than the main vessel has been investigated.

The thermal baffles prevent the main vessels from contacting hot sodium and are constructed of co-axial cylinders which are quite thin with a free top edge and they contain liquid sodium. When they are subjected to seismic loading, the fluid pressure caused by the fluid-structure coupling vibration acts on both their inner and outer surfaces as non-uniformly distributing pressure along the axial direction of the termal baffles [3]. The estimation of the buckling strength of the thermal baffles ordinary requires an equivalent dynamic method. That is, first the pressure distribution is calculated by linear fluid-structuire coupling analysis and the buckling strength is calculated by static buckling analysis using pressure distribution as a static distributed force.

The buckling of liquid storage tanks caused by seismic excitation has been observed and investigated in terms of the bending buckling mode.[4] Their buckling strength is mainly determined by the critical strength required for axial compression. These tanks are taller than thermal baffles and they have clamped or fixed edges. Regarding external pressure buckling, a formula to obtain the buckling strength of thin cylinders under uniform distributing pressure

is available.[5] Still the supporting condition of thermal baffles are not included by the formula. As a result, it is necessary to investigate the buckling of thin short cylindrical shells such as thermal baffles under fluid pressure.

For this purpose, the dynamic buckling experiments of thin cylindrical shells placed inside a rigid liquid containers which represent the thermal baffles and the reactor vessel of FBRs were performed using a shaking table. The buckling mode and the buckling strength were clarified. The buckling pressure based on the experiments is comparable with those obtained from analytical estimates.

2 DYNAMIC BUCKLING EXPERIMENTS

2.1 *Test Apparatus*

Dynamic buckling tests were conducted using the test apparatus shown in Figs. 1 and 2. Test cylinders representing the thermal baffles were placed inside rigid liquid containers representing the main vessel filled with water and they constructed co-axial cylinders. The gap between the test cylinder and the rigid container was 50 mm. The height of the fluid was 300 mm and the top of the test cylinder was 50 mm above the water surface. A shaking table (Fig. 1) was used to apply seismic excitation and the motion of the table simulated that of the supporting point of the thermal baffles of the actual structure. Horizontal vibration was applied to the rigid cylinder suspended from the cantilever by the actuator and fluid pressure due to the vibration of the rigid cylinder acted on the inner wall of the test cylinders. This was the pressure applying test.(Fig. 2)

Three test cylinders made of polyester plate were used. Figure 3 shows the configuration of the test cylinders. One was a co-axial thin cylinder with a narrow gap of 30 mm and the two others were single cylinders. The test cylinders were fixed to a rigid flange at the bottom and the top edge was free. They were 400 mm in radius and 350 mm in height, which corresponds to about one twentieth the size of a demonstration-class tank-type FBR thermal baffles. The ratio of radius to thickness was 400. The initial shape imperfection of the cylinders was found to be less than 0.75% of the diameter. The material properties and the sizes of the cylinders are shown in Table 1.

The types of sensors and their locations are shown in Fig. 4. The displacement at the top of the test cylinders measured by the sensor attached to the inside of the rigid containers and the circumferential strain at the top were used to obtain buckling deformation. The pressure at the flange near the bottom of the cylinders and that at the inner wall of the rigid container were also measured. The pressure sensors were located around the middle circumference and along the axis on shaking direction of the rigid container.

2.2 *Test conditions*

It is important to follow the similarity laws between the prototype structure and test models. However, it is difficult to follow this precisely in a fluid structure coupling system. Despite this, the similarity between the fluid pressure and cylinder elasticity can mainly be maintained and the similarity in the time domain is 1/1.8. As the dynamic pressure applied to the thermal baffles arises as a result of the dominant vibration mode of 6.5Hz for a actual FBR which is obtained as the beam mode vibration of the main vessel, the excitation frequency for the experiments are determined to be 13 Hz. Sinusoidal waves of 13Hz were used. The design seismic input wave for FBR was also used. It was filtered to represent the response wave at the bottom of the thermal baffles. They had the same frequency characteristics corresponding

to the dominant vibration mode of an actual FBR. The response spectrum of input seismic motion is shown in Fig. 5, which is one of the narrow band random waves.

2.3 *Test results*

2.3.1 *Response characteristics*

1) Seismic excitation tests for TP-1

In the dynamic buckling tests, the level of input acceleration was gradually increased. Figures 6 to 8 show the test results for TP-1 under seismic wave excitation. Figure 6 shows the response displacement time history at the top of the cylinders on the shaking direction with various input acceleration levels. Response displacement is amplified depending on the input acceleration level and wave form of response displacement such as the frequency characteristic changes. The relation between input acceleration and response displacement and the pressure measured at the flange is shown in Fig.7. The response displacement suddenly increases when it exceeds 1 mm. Figure 8 shows the pressure and displacement relation. The upper limit for the pressure clearly appears at 1 kPa. The threshold of buckling is the changing point in the pressure and displacement relation.

2) Sinusoidal wave excitation test for TP-1 and TP-2

Results for TP-1 and TP-2 under sinusoidal wave excitation tests are shown in Figs. 9 to 11. Figure 9 shows the time history for the input acceleration, response displacement and the pressure of TP-1. Subharmonic vibration clearly appears in the response displacement when it exceeds about 0.2 mm and the displacement increases with time. However, the pressure at the flange is not affected by subharmonic vibration and it keeps same level. The pressure at the flange represents the strength of the test cylinders. Under seismic wave excitation, subharmonic vibration also occurs as shown by Fig. 6 when the displacement reaches higher than 2 mm. Figures 10 and 11 show the displacement-pressure relation of TP-1 and TP-2 under sinusoidal wave excitation. TP-2 is the pressure applying test and subharmonic vibration is also observed. The pressure at the flange at the threshold of buckling is about 0.6 kPa for both cases and it is smaller than that under seismic wave excitation.

3) Seismic and sinusoidal wave excitation tests for TP-3

The double cylinder model TP-3 requires a higher acceleration level to induce buckling than the single cylinder model TP-1. Subharmonic vibration also occurs under sinusoidal wave excitation, and the threshold for buckling under seismic wave excitation is also higher than that under sinusoidal wave excitation. However, the increase in displacement due to subharmonic vibration is not as severe compared to the response of TP-1. Sudden change does not appear in the acceleration-displacement relation or the pressure-displacement relation under both sinusoidal wave excitation and seismic wave excitation. The experimental results indicated that buckling first occurred in the outer cylinder. It next occurred in the inner one and with the increase in the displacement of the inner cylinder, that of the outer cylinder slowed down. This is because the pressure distribution between the inner and the outer cylinder changed depending on the postbuckling response of both cylinders.

The difference in the buckling pressure will be discussed by examining the vibration mode and the fluid pressure of both the inside and outside of the cylinders.

2.3.2 *Buckling mode*

The buckling mode is shown by Fig. 12 for TP-1 under sinusoidal wave excitation. The number of waves is from 7 to 8 observed by strain distribution. The shaking direction is from 0 degree to 180 degrees. The displacement is 8 mm at 0 degree. Buckling deformation can

clearly be observed when the displacement was growing under subharmonic vibration.

2.3.3 *Pressure distribution*

The axial and circumferential pressure distribution when buckling occurs is shown in Fig. 13. They were measured inside the rigid liquid container. It has almost a cosine θ distribution around the circumference. As a result, it can be said that the fluid pressure inducing buckling under horizontal seismic excitation has a cosine θ distribution. The pressure distribution along the axial direction has a maximum value at the middle height. The shape does not change significantly before or after the buckling.

2.3.4 *Estimation of pressure distribution at the threshold of buckling*

The buckling strength of the cylinders from experimental results was determined by subtracting the fluid pressure of the inside of the cylinders from that outside them. The measured pressure was not enough to determine the pressure distribution of the cylinder surface. Linear fluid-structure coupling vibration FEM analysis was used to interpolate the experimental results. As the acceleration-pressure relation from the experimental results such as shown in Fig. 7 is almost linear before the buckling threshold, we assumpted that the pressure distribution before buckling remains linear.

The model for FEM analyses is shown by Fig. 14. The conditions for FEM analysis represent the test conditions. The pressure from FEM analysis for TP-1 and TP-3 under sinusoidal wave excitation of a small input level is also shown in Fig.14. For TP-1, the fluid pressure at the inner and the outer surface of a cylinder is out of phase. For TP-3, the fluid pressure distribution is more complicated than that of TP-1. This is because the mode of vibration is also more complicated. The fluid pressure of the inner and the outer surface of the outer cylinder is in phase. Therefore, the pressure acting on the cylinder becomes smaller for TP-3 than it does for TP-1 under the same excitation conditions. It can be said from the FEM analysis results that the pressure to which single cylinder model is subjected is distributed to both cylinders of co-axial cylinder model. Because the pressure distribution of TP-3 is complicated as shown by Fig. 14, the vibration mode must be examined carefully.

The fluid pressure acting on the cylinder is obtained by subtracting that of the inside of the cylinders from that of the outside using linear FEM analysies results. The fluid pressure distribution at the threshold of buckling is determined by comparing the measured acceleration and measured pressure at the threshold of buckling with the analysis results. The buckling pressure thus obtained for TP-1 ,TP-2 and TP-3 is shown by Fig. 15. Fluid pressure which depends on the vibration mode distributes non-uniformly along the axial direction of the cylinders. The buckling pressure for TP-1 under seismic wave excitation is larger than those for TP-1 and TP-2 under sinusoidal wave excitation. The buckling pressure of TP-3 under seismic wave excitation is smaller than the others. This is because the vibration mode of TP-3 is more complicated than that of the single cylinder model and a little difference in the vibration mode affects the pressure distribution. This is also because the threshold of buckling does not appear clearly in the acceleration-displacement relation, or the displacement-pressure relation for TP-3 compared with the single cylinder model. The threshold of buckling has been determined conservatively from this reason.

The buckling pressure was determined as shown in Table 2. The pressure is indicated by the maximum value among the axial distribution. The acceleration and the displacement at the threshold of buckling is also shown. We also found that;

1) The acceleration of single cylinder models such as TP-1 and TP-2 is smaller than that of TP-3 because of the difference in the pressure acting on the cylinder as revealed by Fig.

14.

2) The buckling pressure under sinusoidal wave excitation is smaller than that under seismic wave excitation for both the single cylinder model TP-1 and the double cylinder model TP-3. This may be due to the effect of subharmonic vibration.
3) The determination of fluid pressure using linear fluid-structure coupling vibration analysis requires a precise estimation of the vibration mode.

3 DISCUSSION

3.1 *Analytical evaluation of the buckling strength under fluid pressure*

The buckling pressure obtained from the experiments was compared to the analytical value. Equivalent static buckling analysis was usually used. Buckling strength was calculatied by substituting the fluid pressure as a static distributing force and applying it on the shell. The fluid pressure distribution along the cylinder axis was determined beforehand by linear analysis as shown by Fig. 15. The fluid pressure distribution around the circumferece was supposed to have a cosine θ distribution. Buckling analysis was done using the ABAQUS code and the AXIS code which were specially developed for the FBR structure. [6]

An example of the model for static analysis is shown in Fig. 16. The initial imperfection in the shape of the cylinder was considered to be about 5 mm at maximum. The buckling mode is shown in Fig. 17. Buckling deformation mainly appears on the side where the pressure acts as external pressure. On the other side, the pressure acts as internal pressure. Buckling deformation thus appears locally and is similar to that observed in the experiments. The pressure-dispacement relation is shown in Fig. 18. On the external pressure loading side, the displacement advances against the direction of the pressure loading. The buckling pressure from static analysis is determined at the upper limit value of pressure in the displacement-pressure relation.

The experimental results and analytical ones are compared for TP-1 in Fig. 19. The analytical buckling pressure for a model with no initial shape imperfection is also shown. This is calculated by buckling eigenvalue analysis using same pressure distribution. The analytical buckling pressure reduces by considering the initial shape imperfection. Comparing the experimental and analytical results, they well agree and the difference between them is no larger that 30%. The reduction in buckling pressure due to subharmonic vibration can be explained by considering the initial shape imperfection in the analysis.

The buckling pressure obtained during the experiments are compared with the analytical values summarized by Table 3. In Table 3, the buckling pressure is shown as a maximum value along the axial direction. From Table 3, we can see that;

1) The buckling mode predicted by analysis agrees with that obtained by the experiments.
2) The experimental buckling pressure almost agrees with the analysies results except for TP-3 under sinusoidal wave excitation.
3) The effect of amplification in response displacement due to subharmonic vibration can be explained by considering initial shape imperfection in static buckling analysis.
4) For the double cylinder TP-3 model, the buckling pressure from experiments is smaller than analytical value. The reason is that the estimation of the vibration mode in linear analysis requires more precision and that The determination of the occurrence of the buckling for TP-3 is conservative.

3.2 *The effect of subharmonic vibration*

Subharmonic vibration was observed under the sinusoidal wave excitation of polyester cylinders. The same phenomena was observed and reported by Chiba [7] as parametoric vibration. It appears when the displacement exceeds 0.2 mm. When the response displacement reaches 1 mm, it suddenly grows. Subharmonic vibration accompanies the oval vibration of cylinders. Figure 20 shows the tapping test results for TP-1. Many oval vibration modes exist and there is a lowest mode near 6.9 Hz. The oval vibration modes of 6.9 Hz and 7.5 Hz is shown. The number of waves is supposed to be 8 for the 6.9Hz mode and 7 for the 7.5Hz mode. These agree with the buckling mode shown in Fig. 12. Thist is supposed to be the same mode which was observed as subharmonic excitation under 13 Hz sinusoidal wave excitation.

Based on the experimental results, subharmonic vibration scarcely occurs under seismic wave excitation. Also the buckling strength predicted by analysis agrees with the experimental results including that obtained under subharmonic excitation. From the seismic design point of view, it seems reasonable to say that the effect of the subharmonic vibration is not very serious under seismic wave excitation. Still it is necessary to estimate the conditions and the effect of subharmonic vibration.

4 BUCKLING ESTIMATION FOR ACTUAL FBR THERMAL BAFFLES

The buckling strength of the demonstration-class loop-type FBR model was estimated. The model is shown in Fig. 21. The main vessel is about 10 m in diameter and three thermal baffles were modeled. The thickness of the thermal baffles changed from 15mm to 20mm and the gap between each of them or between the thermal baffle and the main vessel was about 40 mm.

First, fluid-structure coupling linear vibration analysis was done using designed seismic waves. The material property used was SUS304 at 500 degrees. The pressure distribution of each fluid region was calculated by time response method. The pressure distribution of each thermal baffle was obtained by subtracting the pressure on the inside and the outside as shown in Fig. 22. The pressure distributes non-uniformly along the axial direction of each thermal baffle and the shape of it varies depending on the vibration mode.

Static buckling analysis was performed using representative pressure distribution which had a maximum value. The buckling mode is shown in Fig. 23. It is also external buckling mode. The buckling is elastic buckling. The buckling strength is 70% of the predicted value of pressure obtained by fluid-structure coupling analysis using designed seismic wave excitation.

As indicated by Fig. 22, the pressure distribution makes difference depending on the structural conditions and on the input seismic waves. It is important to investigate the dependence of buckling strength on the shape of the pressure distribution. Terefore, the buckling strength for four kinds of representative pressure distributions was compared. One was obtained from fluid-structure coupling analysis for the FBR model. The others were Housner distribution, uniform distribution and static hydropressure distribution. Buckling analyses was done using eigenvalue buckling analysis. The buckling pressures were compared and are shown in Fig. 23. Buckling strength depends on the pressure distribution. In comparing the maximum values of all pressure shapes, the uniform pressure is the severest. The pressure acting near the fixed edge of the cylinder has little effect on the buckling strength. The buckling pressure is determined by the pressure acting on the upper part of the cylinder. Consequently, it is necessary to calculate buckling strength when the shape of the

pressure distribution changes. From the design point of view, the further study is required to obtain a simple evaluation method or formula for buckling strength of the thermal baffles.

5 CONCLUSION

Dynamic buckling tests using fluid-filled thin cylinders with a free edge representing the thermal baffle of a tank-type FBR were performed.

1) The buckling strength and the buckling mode under dynamic fluid pressure with different cylinder models and different excitation conditions were clarified.
2) The buckling mode and the buckling strength predicted by static analyses agreed with the experimental results.
3) An equivalent dynamic analytical method to estimate buckling strength impling that pressure distribution can be predicted by linear fluid-structure coupling analysis and buckling strength can be predicted by static buckling analyses was revealed to be available.
4) Subharmonic vibrations were observed under the sinusoidal wave excitation of a particular frequency andthis reduced buckling strength. Still the reduction in buckling strength due to subharmonic vibration can be estimated by static buckling analyses.
5) The pressure distribution at the buckling strength of a demonstration FBR were analytically estimated.
6) The buckling strength depends on the shape of the pressure distribution. Further study is required to obtain a simple method to evaluate buckling strength.

This study is carried out as part of a project commissioned by the Ministry of International Trade and Industry, entitled "Verification Tests of Fast Breeder Reactor Technology", which has began in 1987.

References

1. Akiyama, H. et al., 1995, "Outline of the seismic buckling design guideline of FBR main vessels", 13th SMiRT, Vol. E, pp .445-456.
2. Matsuura, S. et al., 1995," Shear-bending buckling strength of FBR main vessels", 13th SMiRT, Vol.E, pp .457-462
3. Brochard, A. et al., 1983, "Dynamic buckling of fluid-coupled cylinders" , 7th SMiRT,Vol. E, pp .243-249
4. Niwa, A. and Clough, W., 1982, "Buckling of cylindrical liquid-storage tanks under earthquake loading", Earthquake engineering and structural dynamics, Vol 10, pp. 107-122
5. Yamaki, N., 1984, "Elastic stability of circular cylindrical shells", North-Holland.
6. Ohtsubo, H., et al., 1995, " Elastic-plastic dynamic buckling analyses for FBR main vessels", PVP-Vol. 300, Dynamic Fracture, Failure, and Deformation, pp. 129-136
7. Chiba, M. et al., 1986, "Dynamic Stability of Liquid-filled Cylindrical Shells under Horizontal Excitation, Part I : Experiment", Journal of Sound and Vibration Vol. 104-2, pp. 301-319

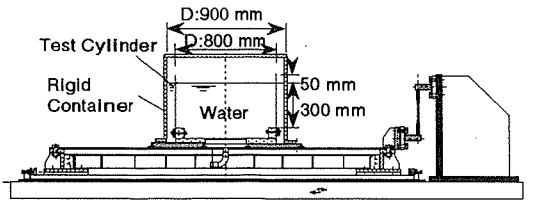

Fig. 1 Shaking table test apparatus

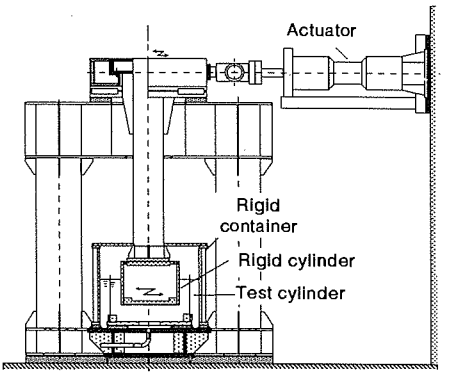

Fig. 2 Pressure applying test apparatus

Table 1 Test cylinder features

No.	Model	Material	Radius [mm]	Height [mm]	Thickness [mm]	Young's Modulus [GPa]
TP-1	Single	Polyester	400	350	1	1.54
TP-2	Single	Polyester	400	350	1	1.54
TP-3	Double	Polyester	400	350	1	1.54

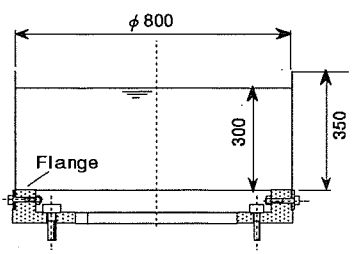

(1) Single cylinder structure

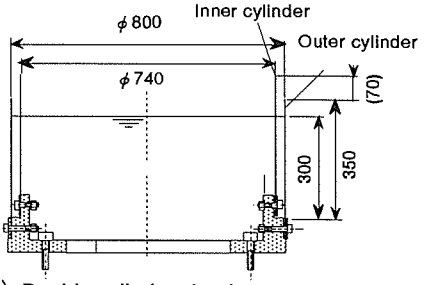

(2) Double cylinder structure

Fig. 3 Test cylinder structures

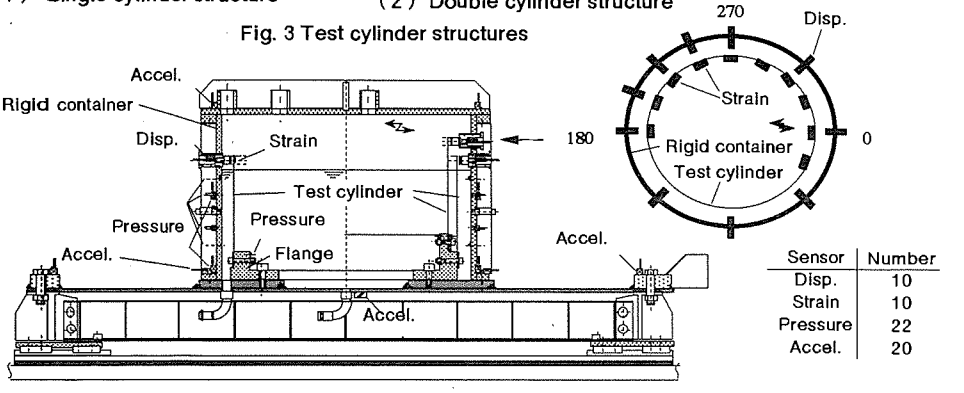

Sensor	Number
Disp.	10
Strain	10
Pressure	22
Accel.	20

Fig. 4 Types of sensors and locations

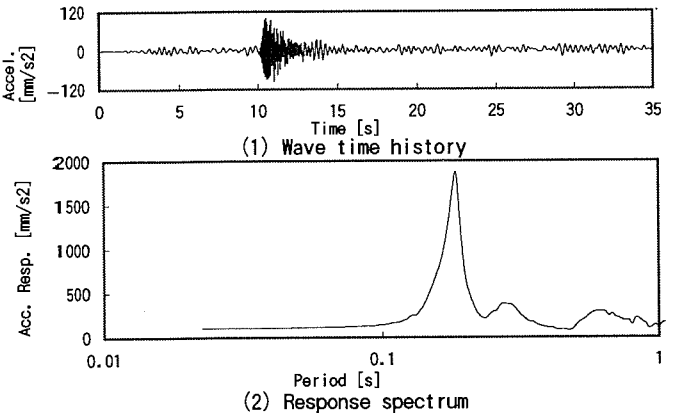

Fig. 5 Design seismic wave at the bottom of the thermal baffles

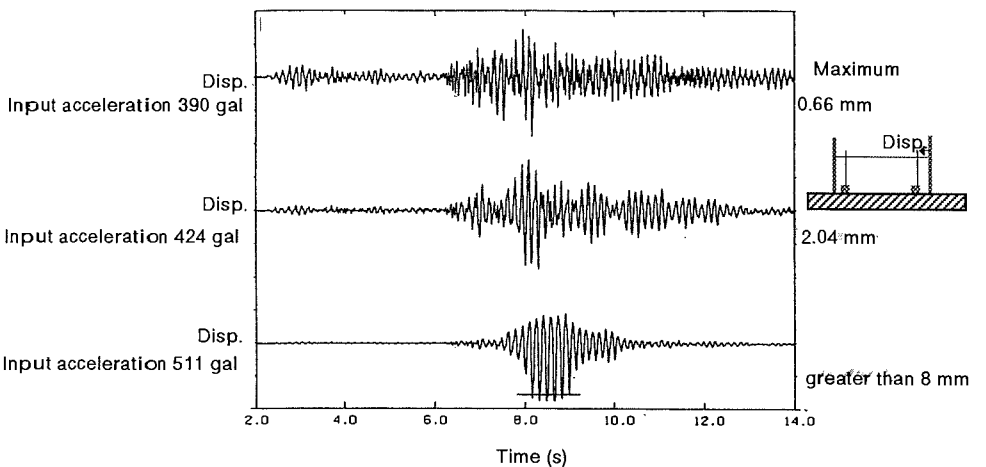

Fig. 6 Displacement time history with various acceleration levels

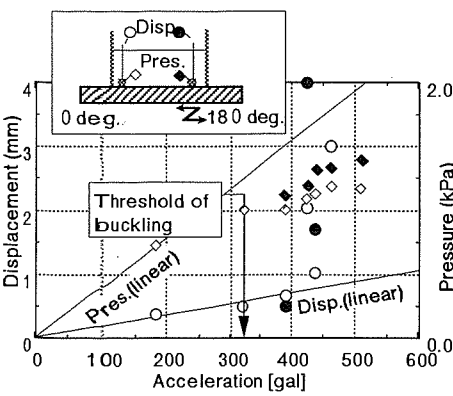

Fig. 7 Acceleration and displacement, pressure relation

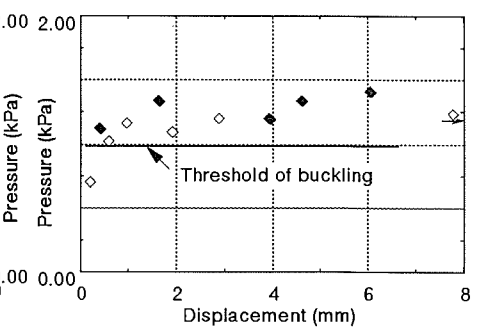

Fig. 8 Pressure and displacement relation

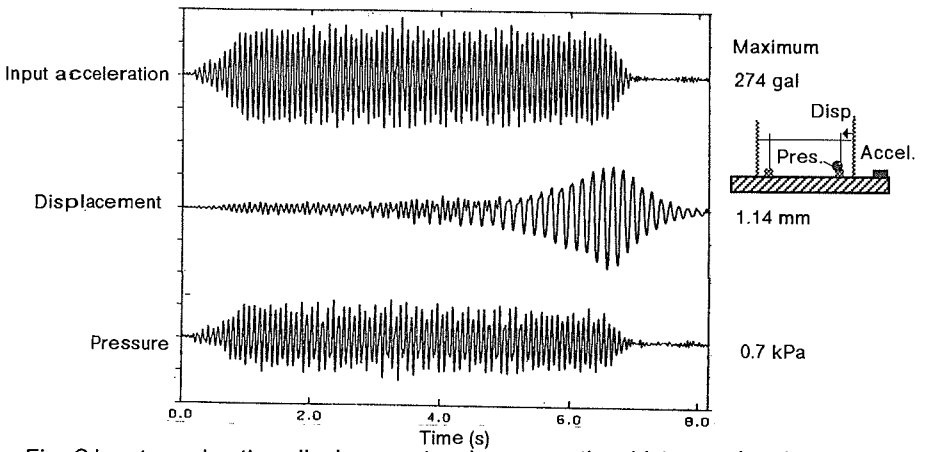

Fig. 9 Input acceleration, displacement and pressure time history under sinusoidal wave excitation/TP-1

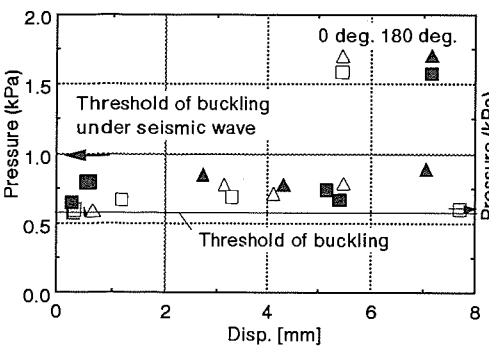

Fig. 10 Pressure and displacement relation (TP-1/under sine wave excitation)

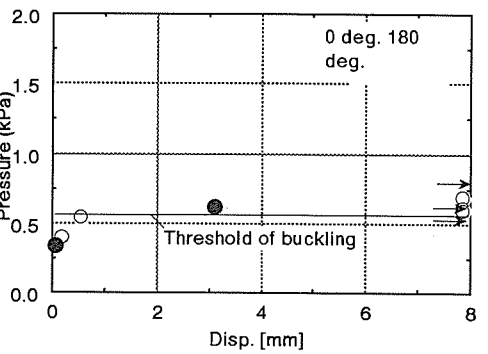

Fig. 11 Pressure and displacement relation (TP-2/under sine wave excitation)

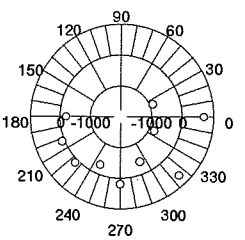

Fig.12 Buckling mode

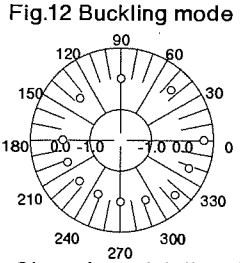

(1) Circumferential direction

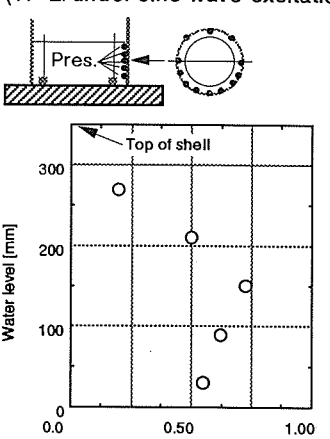

(2) Axial direction

Fig. 13 Pressure distribution

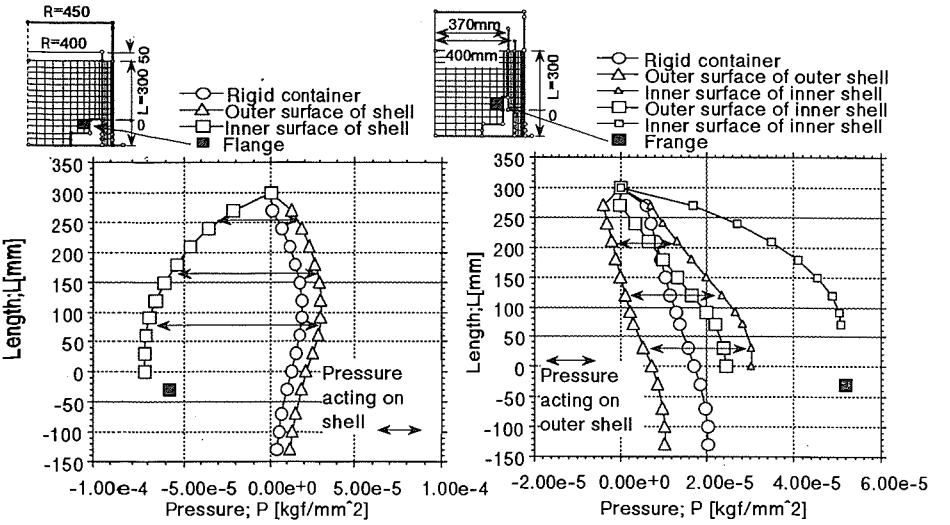

(1) TP-1 under sinusoidal wave of 200gal (1) TP-3 under sinusoidal wave of 200gal

Fig. 14 Pressure distribution from FSI analyses

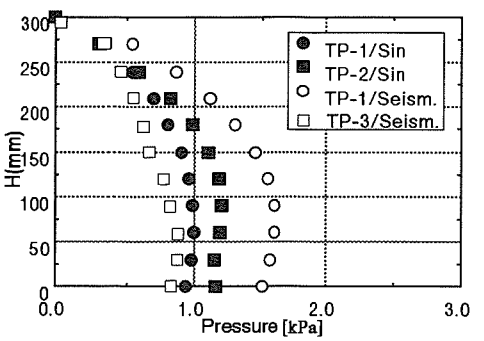

Fig.15 Pressure distribution at the buckling

Table 2 Response at the threshold of buckling

Model	Wave	Accel. [gal]	Disp. [mm]	Pressure [kPa]
TP-1	Sin	230	0.70	1.0
TP-1	Seism.	320	0.50	1.6
TP-2	Sin.	300	0.60	1.2
TP-3	Sin.	320	0.60	0.4
TP-3	Seism.	700	0.80	0.8

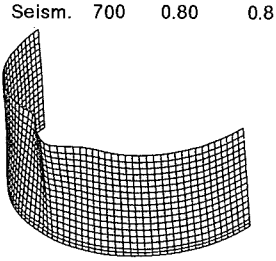

Fig. 16 Static buckling analyses model

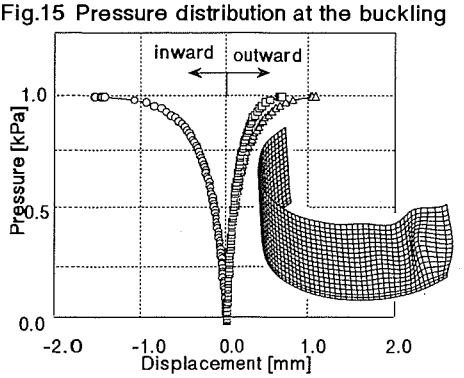

Fig. 18 Pressure-displacement relation from static analyses

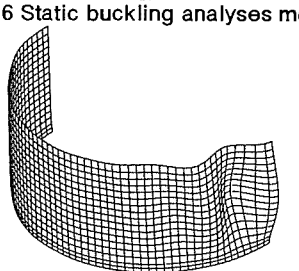

Fig. 17 Buckling deformation from static analyses

Table 13 Comparison of buckling pressure

Model	Wave	Pressure at buckling		
		Experiments [kPa]	Analyses	
			with imp. [kPa]	no imp. [kPa]
TP-1	Sin	1.0	1.00	1.20
TP-1	Seism.	1.6		
TP-2	Sin	1.2	0.90	1.10
TP-3	Sin	0.4	0.90	1.10
TP-3	Seism.	0.8		

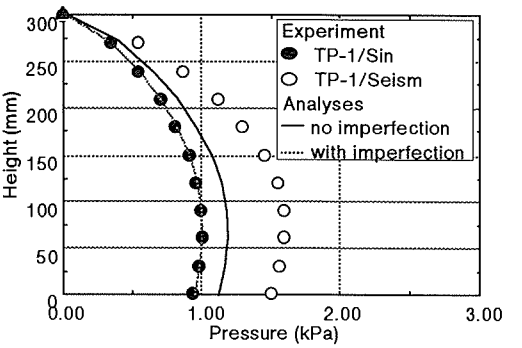

Fig. 19 Comparison of buckling pressure

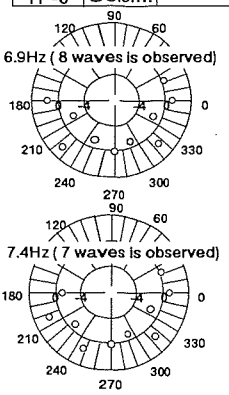

(1) Oval vibration mode

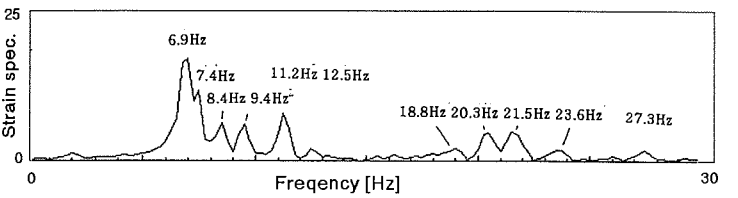

(2) Spectrum

Fig. 20 Tapping test results

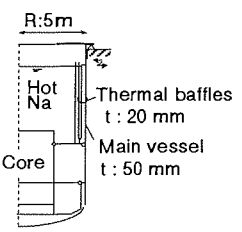

Fig. 21 Loop type FBR model

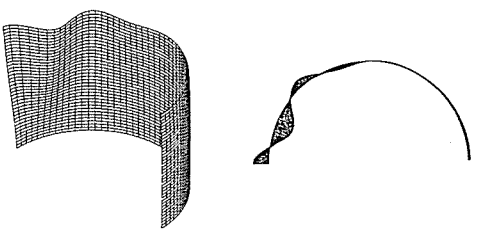

Fig. 23 Buckling mode

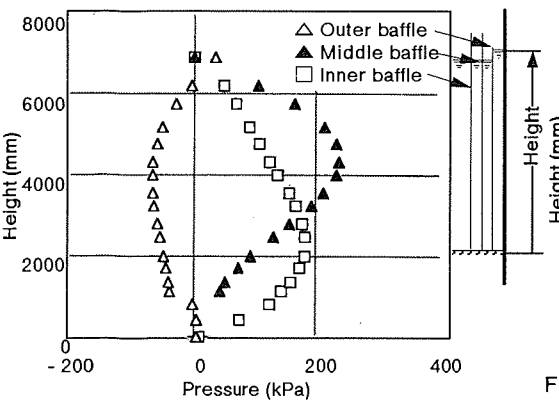

Fig. 22 Pressure distribution

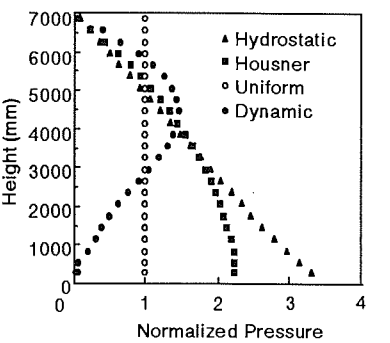

Fig. 24 Dependence of buckling strength on pressure distribution